

UC Davis

UC Davis Previously Published Works

Title

Wavefront correction and high-resolution in vivo OCT imaging with an objective integrated multi-actuator adaptive lens

Permalink

<https://escholarship.org/uc/item/1899m4st>

Journal

Optics Express, 23(17)

ISSN

1094-4087

Authors

Bonora, Stefano
Jian, Yifan
Zhang, Pengfei
[et al.](#)

Publication Date

2015-08-24

DOI

10.1364/oe.23.021931

Peer reviewed

Wavefront correction and high-resolution *in vivo* OCT imaging with an objective integrated multi-actuator adaptive lens

Stefano Bonora,^{1,2,6,7} Yifan Jian,^{3,6} Pengfei Zhang,⁴ Azhar Zam,⁴ Edward N. Pugh, Jr.⁴
Robert J. Zawadzki,^{4,5,8} and Marinko V. Sarunic³

¹CNR-Institute for Photonics and Nanotechnology, Via Trasea 7, 35131, Padova, Italy

²Hilase project, Institute of Physics AS CR v.v.i., Na Slovance 2, 18221, Prague, Czech Republic

³School of Engineering Science, Simon Fraser University, Burnaby, BC, V5A1S6, Canada

⁴UC Davis RISE Small Animal Ocular Imaging Facility, Department of Cell Biology and Human Anatomy,
University of California Davis, Davis, CA 95616, USA

⁵Vision Science and Advanced Retinal Imaging laboratory (VSRI), Department of Ophthalmology & Vision Science,
University of California Davis, Sacramento, CA 95817, USA

⁶S. Bonora and Y. Jian contributed equally to this work.

⁷stefano.bonora@dei.unipd.it

⁸rjzawadzki@ucdavis.edu

Abstract: Adaptive optics is rapidly transforming microscopy and high-resolution ophthalmic imaging. The adaptive elements commonly used to control optical wavefronts are liquid crystal spatial light modulators and deformable mirrors. We introduce a novel Multi-actuator Adaptive Lens that can correct aberrations to high order, and which has the potential to increase the spread of adaptive optics to many new applications by simplifying its integration with existing systems. Our method combines an adaptive lens with an imaged-based optimization control that allows the correction of images to the diffraction limit, and provides a reduction of hardware complexity with respect to existing state-of-the-art adaptive optics systems. The Multi-actuator Adaptive Lens design that we present can correct wavefront aberrations up to the 4th order of the Zernike polynomial characterization. The performance of the Multi-actuator Adaptive Lens is demonstrated in a wide field microscope, using a Shack-Hartmann wavefront sensor for closed loop control. The Multi-actuator Adaptive Lens and image-based wavefront-sensorless control were also integrated into the objective of a Fourier Domain Optical Coherence Tomography system for *in vivo* imaging of mouse retinal structures. The experimental results demonstrate that the insertion of the Multi-actuator Objective Lens can generate arbitrary wavefronts to correct aberrations down to the diffraction limit, and can be easily integrated into optical systems to improve the quality of aberrated images.

©2015 Optical Society of America

OCIS codes: (220.1080) Active or adaptive optics; (110.4500) Optical coherence tomography.

References and links

1. R. Ragazzoni, E. Marchetti, and G. Valente, "Adaptive-optics corrections available for the whole sky," *Nature* **403**(6765), 54–56 (2000).
2. N. Ji, D. E. Milkie, and E. Betzig, "Adaptive optics via pupil segmentation for high-resolution imaging in biological tissues," *Nat. Methods* **7**(2), 141–147 (2010).
3. C. Dainty, *Adaptive Optics for Industry and Medicine: Proceedings of the Sixth International Workshop* (Imperial College Press, 2008).
4. R. Tyson, *Adaptive Optics Engineering Handbook* (CRC Press, 1999).
5. A. F. Naumov and G. Vdovin, "Multichannel liquid-crystal-based wave-front corrector with modal influence functions," *Opt. Lett.* **23**(19), 1550–1552 (1998).

6. A. F. Naumov, M. Y. Loktev, I. R. Guralnik, and G. Vdovin, "Liquid-crystal adaptive lenses with modal control," *Opt. Lett.* **23**(13), 992–994 (1998).
7. D. Graham-Rowe, "Liquid lens make a splash," *Nat. Photonics*, **2006**, 2–4 (2006).
8. H. Ren and S.-T. Wu, "Variable-focus liquid lens by changing aperture," *Appl. Phys. Lett.* **86**(21), 211107 (2005).
9. L. Dong, A. K. Agarwal, D. J. Beebe, and H. Jiang, "Adaptive liquid microlenses activated by stimuli-responsive hydrogels," *Nature* **442**(7102), 551–554 (2006).
10. F. Schneider, D. Eberhard, D. Strohmeier, C. Muller, and U. Wallrabe, "Adaptive Fluidic PDMS-Lens with integrated piezoelectric actuator," *IEEE 21st International Conference on Micro Electro Mechanical Systems, MEMS 2008*, 120–123 (2008).
11. G. D. Love, D. M. Hoffman, P. J. W. Hands, J. Gao, A. K. Kirby, and M. S. Banks, "High-speed switchable lens enables the development of a volumetric stereoscopic display," *Opt. Express* **17**(18), 15716–15725 (2009).
12. S. Shian, R. M. Diebold, and D. R. Clarke, "Tunable lenses using transparent dielectric elastomer actuators," *Opt. Express* **21**(7), 8669–8676 (2013).
13. F. Carpi, G. Frediani, S. Turco, and D. De Rossi, "Bioinspired tunable lens with muscle-like electroactive elastomers," *Adv. Funct. Mater.* **21**(21), 4152–4158 (2011).
14. A. Mermillod-Blondin, E. McLeod, and C. B. Arnold, "High-speed varifocal imaging with a tunable acoustic gradient index of refraction lens," *Opt. Lett.* **33**(18), 2146–2148 (2008).
15. I. Grulkowski, K. Szulzycki, and M. Wojtkowski, "Microscopic OCT imaging with focus extension by ultrahigh-speed acousto-optic tunable lens and stroboscopic illumination," *Opt. Express* **22**(26), 31746–31760 (2014).
16. I. Grulkowski, D. Jankowski, and P. Kwiek, "Acousto-optic interaction of a Gaussian laser beam with an ultrasonic wave of cylindrical symmetry," *Appl. Opt.* **46**(23), 5870–5876 (2007).
17. Y. Jian, J. Xu, M. A. Gradowski, S. Bonora, R. J. Zawadzki, and M. V. Sarunic, "Wavefront sensorless adaptive optics optical coherence tomography for in vivo retinal imaging in mice," *Biomed. Opt. Express* **5**(2), 547–559 (2014).
18. R. J. Zawadzki, S. S. Choi, S. M. Jones, S. S. Oliver, and J. S. Werner, "Adaptive optics-optical coherence tomography: optimizing visualization of microscopic retinal structures in three dimensions," *J. Opt. Soc. Am. A* **24**(5), 1373–1383 (2007).
19. G. Vdovin, O. Soloviev, A. Samokhin, and M. Loktev, "Correction of low order aberrations using continuous deformable mirrors," *Opt. Express* **16**(5), 2859–2866 (2008).
20. S. Bonora and L. Poletto, "Push-pull membrane mirrors for adaptive optics," *Opt. Express* **14**(25), 11935–11944 (2006).
21. D. R. Williams, "Imaging single cells in the living retina," *Vision Res.* **51**(13), 1379–1396 (2011).
22. A. Roorda, "Adaptive optics for studying visual function: a comprehensive review," *J. Vis.* **11**(7), 6 (2011).
23. J. Carroll, D. B. Kay, D. Scoles, A. Dubra, and M. Lombardo, "Adaptive optics retinal imaging—clinical opportunities and challenges," *Curr. Eye Res.* **38**(7), 709–721 (2013).
24. Y. Jian, R. J. Zawadzki, and M. V. Sarunic, "Adaptive optics optical coherence tomography for in vivo mouse retinal imaging," *J. Biomed. Opt.* **18**(5), 056007 (2013).
25. M. J. Booth, "Wavefront sensorless adaptive optics for large aberrations," *Opt. Lett.* **32**(1), 5–7 (2007).
26. Y. Geng, L. A. Schery, R. Sharma, A. Dubra, K. Ahmad, R. T. Libby, and D. R. Williams, "Optical properties of the mouse eye," *Biomed. Opt. Express* **2**(4), 717–738 (2011).
27. Y. Geng, A. Dubra, L. Yin, W. H. Merigan, R. Sharma, R. T. Libby, and D. R. Williams, "Adaptive optics retinal imaging in the living mouse eye," *Biomed. Opt. Express* **3**(4), 715–734 (2012).
28. G. Palczewska, Z. Dong, M. Golczak, J. J. Hunter, D. R. Williams, N. S. Alexander, and K. Palczewski, "Noninvasive two-photon microscopy imaging of mouse retina and retinal pigment epithelium through the pupil of the eye," *Nat. Med.* **20**(7), 785–789 (2014).
29. M. Zacharria, B. Lamory, and N. Chateau, "Biomedical imaging: New view of the eye," *Nat. Photonics* **5**(1), 24–26 (2011).
30. K. S. K. Wong, Y. Jian, M. Cua, S. Bonora, R. J. Zawadzki, and M. V. Sarunic, "In vivo imaging of human photoreceptor mosaic with wavefront sensorless adaptive optics optical coherence tomography," *Biomed. Opt. Express* **6**(2), 580–590 (2015).
31. N. Doble, D. T. Miller, G. Yoon, and D. R. Williams, "Requirements for discrete actuator and segmented wavefront correctors for aberration compensation in two large populations of human eyes," *Appl. Opt.* **46**(20), 4501–4514 (2007).

1. Introduction

Adaptive Optics (AO) is a well-established branch of optics that is contributing to important advancements in many different fields of science, including astronomy, microscopy, ophthalmology, vision science, laser beam shaping and coherent control, and atmospheric propagation. (See for example [1] or more recently [2]. For a comprehensive review of applications, [3]). Nonetheless the dissemination of AO is still limited by its complexity. Devices that have been used to control the wavefront of a light beam are, in most cases, deformable mirrors that can be actuated by different kinds of forces, including electrostatic,

piezoelectric, electromagnetic etc [4]. The introduction of deformable mirrors into optical systems necessitates the creation of folded optical paths, and the use of wavefront sensors can make its integration impractical, precluding its use in some applications. For this reason refractive wavefront correctors have found interesting applications, as for example in the case of spatial light modulators based on liquid crystals panels. High order aberration control has been extensively demonstrated [2]. Unfortunately, the use of liquid crystal devices has been limited mainly to low power laser applications because they are polarization sensitive and monochromatic [5,6].

Recently, several efforts have been reported on the realization of adaptive lenses. In particular, modulation of the focal length of a lens has been demonstrated with several different technologies. Liquid lenses are very promising in terms of optical power modulation, miniaturization and use of low voltages [7], and are well suited for exploitation in consumer applications. Other examples of adaptive lenses make use of different actuator stimuli or smart materials, including reconcentration distribution [8], hydrogels [9], piezoelectric pump chamber [10], polarization modulation [11], dielectric elastomers [12], bioinspired mimicry of the human eye's accommodation [13] and acousto-optic modulation [14–16]. Although such lenses provide examples of successful refractive devices, they generally cannot correct higher order aberrations. An adaptive lens that can correct for high order aberrations could significantly enlarge the list of possible applications of adaptive optics.

In this paper, we present a Multi-actuator Adaptive Lens (M-AL) that can correct for arbitrary aberrations. To demonstrate its potential we integrated the M-AL into the objective of a high resolution OCT system and acquired *in vivo* mouse retina images, correcting aberrations with a wavefront-sensorless algorithm controlling the M-AL. A significant advantage of transmissive adaptive lenses is that they can be more readily integrated with a range of existing imaging systems. Unlike conventional reflective adaptive optics mirrors, which requires optical setups to relay the pupil plane with folded optical paths, an adaptive lens can be placed in conjunction with the objective for aberration-corrected imaging.

The Multi-actuator Adaptive Lens can correct up to the 4th radial order of Zernike polynomials, without any obstructions (electrodes and actuators) placed inside its clear aperture. The performance of the adaptive lens was characterized using a Shack-Hartmann wavefront sensor for closed loop wavefront measurement and correction, and the effects on images acquired in a wide field microscope configuration are presented.

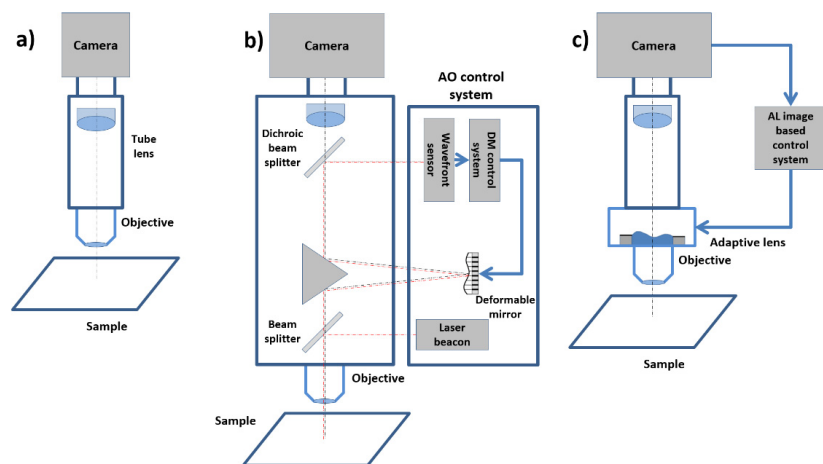


Fig. 1. Integration of adaptive optics with existing imaging systems. a) scheme of a generic imaging system; b) implementation of a closed-loop adaptive optics system with a deformable mirror on the system of panel a). c) Concept of the adaptive optics system based on the integration of the M-AL and an image-based control algorithm.

In addition, we demonstrate that the combination of the Multi-actuator Adaptive Lens with an image-based control algorithm leads to a new method of integrating adaptive optics with imaging systems. The concept is illustrated in Fig. 1 as applied in principle to a generic imaging system [Fig. 1(a)]. [Fig. 1(b)] shows the implementation of state-of-the-art closed loop adaptive optics based on the use of a deformable mirror and a wavefront sensor. The integration of the latter components with existing optical systems is, in most cases, inconvenient or impossible because of the need of relay optics to accommodate the reflective deformable element, or because the use of a beacon for the wavefront sensing is not always possible [17,18]. In contrast, as illustrated in [Fig. 1(c)], the M-AL can be implemented in a generic optical system simply by the addition of the adaptive lens to the objective lens.

2. Methods

2.1 Multi-actuator adaptive lens

The M-AL is composed of two thin glass windows (thickness 150 μm), upon each of which is mounted a piezoelectric actuator ring (see Fig. 2). The space in between the windows is filled with a transparent liquid, mineral oil. The first window is used to generate defocus and astigmatism while the second one generates coma and secondary astigmatism. The piezoelectric actuators have an external diameter of 25 mm and an internal diameter of 10 mm with a thickness of 200 μm . Both rings are divided into 8 sectors that can be actuated independently. The piezo rings are glued to the windows and act as a bimorph actuator, such that the application of a voltage generates a bending of the glass window. The actuators are controlled by a 16 channel high voltage (± 125 V) driver.

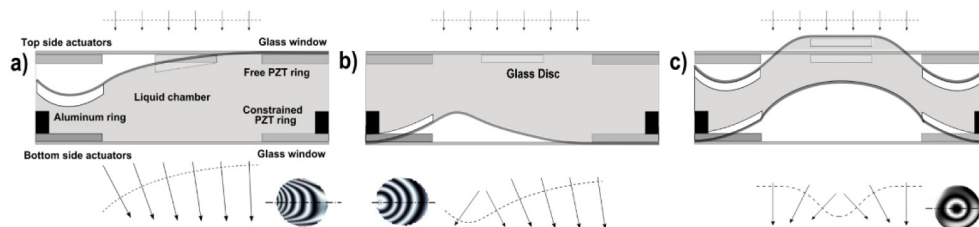


Fig. 2. Layout of the Multi-actuators Adaptive Lens. Panel a-c) show the measured wavefront deformations (arrows) and the interferograms relative to the actuation of the M-AL in three different configurations: a) one electrode on the top window, b) one electrode on the bottom window, c) all the actuators poked with the same voltage value.

The 8 actuators on the top and bottom windows generate different effects because the top window is attached to the actuator by an elastomer foam that is free to move. To generate aberrations up to the 4th order it is necessary to have at least 15 actuators and a ring of actuators outside the active region [1,19,20]. The bottom window is blocked at its border by a rigid aluminum ring that defines the direction of the tangent of the piezoelectric ring. This constraint moves the maximum (or the minimum) of the deformation inside the clear aperture (see [Fig. 2(b)]). Thus each actuator, although placed outside the clear aperture, acts as though it pushes the window from the inside. The shape of the top window is restrained in the center by gluing a transparent disc of borosilicate glass (diameter 3mm, 1mm thick, $n = 1.474$, see [Fig. 2(b)]) with the same refractive index as the liquid (for oil absorption and dispersion properties see NIST website: Mineral Oil, NIST, Standard Reference Material 1922).

Deformation of the surfaces of the adaptive lens are illustrated in Fig. 2. [Fig. 2(c)] shows the effect on the wavefront when a positive voltage is applied to all the actuators; both the windows bend upward, hence the resultant wavefront is compensated everywhere in the aperture except in the center, where the glass disc stiffens the window. Therefore the resultant wavefront presents a peak in the center. Examples of wavefront deformation measured with a wavefront sensor are illustrated in the lower insets of [Figs. 2(a)-2(c)].

The total wavefront deformation can be calculated from the optical path length at each point of the aperture (x,y) , and is given by the difference of the shape of the two windows ($L_1(x,y)$ for the top window and $L_2(x,y)$ for the bottom window) multiplied by the refractive index of the liquid contained in the lens:

$$wf(x,y) = \frac{2\pi}{\lambda} n [L_1(x,y) - L_2(x,y)] = \frac{2\pi}{\lambda} n \left[\sum_1^8 e_{1i}(x,y) c_{1i} - \sum_9^{16} e_{2i}(x,y) c_{2i} \right], \quad (1)$$

where the shape of each window is approximated by the algebraic sum of the deformation of each single electrode in both windows $e_{1/2i}(x,y)$ weighted by its control value $c_{1/2i}$ ($c_{1/2i} = -1$ when the voltage is -125 V and $c_{1/2i} = +1$ when the voltage is $+125$ V).

2.2 Multi-actuator adaptive lens characterization

In order to assess the performance of the M-AL we carried out two tests: the generation of aberrations up to the 4th order Zernike polynomial, and the correction of aberrations in an infinity-conjugated microscope. Details about the experimental setup, combining an infinity conjugated optical microscope with wavefront sensing are reported in Fig. 3.

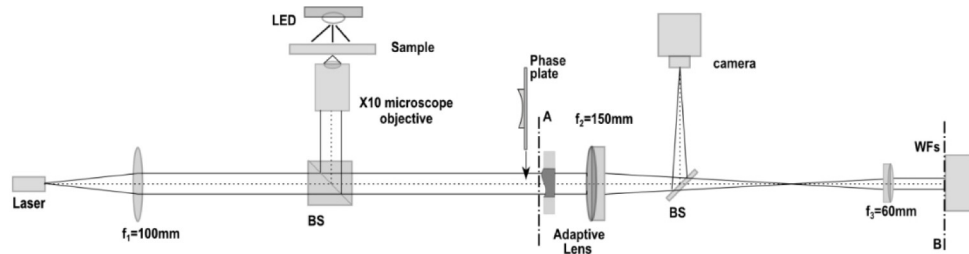


Fig. 3. Experimental layout. BS beam splitter, Wfs wavefront sensor, $f_1 = 100$ mm, $f_2 = 150$ mm, $f_3 = 60$ mm. Plane A (adaptive lens) and B (Wfs) are optically conjugated.

The microscope consisted of a 10X APO-PLAN objective with focal length of 18 mm, and an achromatic doublet (f_1) tube lens with focal length 150 mm, providing a magnification of 8.3x. In order to perform the wavefront correction, the M-AL was placed adjacent to the tube lens, and a collimated laser source (diode laser 667 nm, 1 mW) was co-propagated in the microscope light path. The laser beam was reduced in diameter to 4 mm to enter the aperture of a Shack-Hartmann wavefront sensor by a telescope ($M = 0.4$) composed of achromatic doublet lenses.

The wavefront was controlled in closed loop after the acquisition of the influence functions (i.e. deformation of the wavefront after the actuation of each single actuator), followed by the calculation of the M-AL control voltages [1]. In its neutral position, the M-AL has some aberrations due mainly to the initial flatness of the windows of the adaptive lens; its rms value of 0.25 waves includes mainly astigmatism (Z_{20} , Z_{2-2}) and spherical aberration (Z_{40}). Therefore, the first step in operating the microscope is to correct for the system aberrations: switching to the closed loop, the initial aberration was corrected to 0.042 waves RMS, well below the Marechal criterion ($\lambda/14$) [1]. In making this correction for initial M-AL aberration and the system aberrations, the adaptive lens used $\sim 25\%$ rms of its dynamic range, thus preserving substantial potential for additional corrections. Measurements of the dynamic behavior indicate that the lens has three main resonant peaks at 554 Hz, 2560 and 3000 Hz, indicating that its corrections can be updated a few hundred times per second.

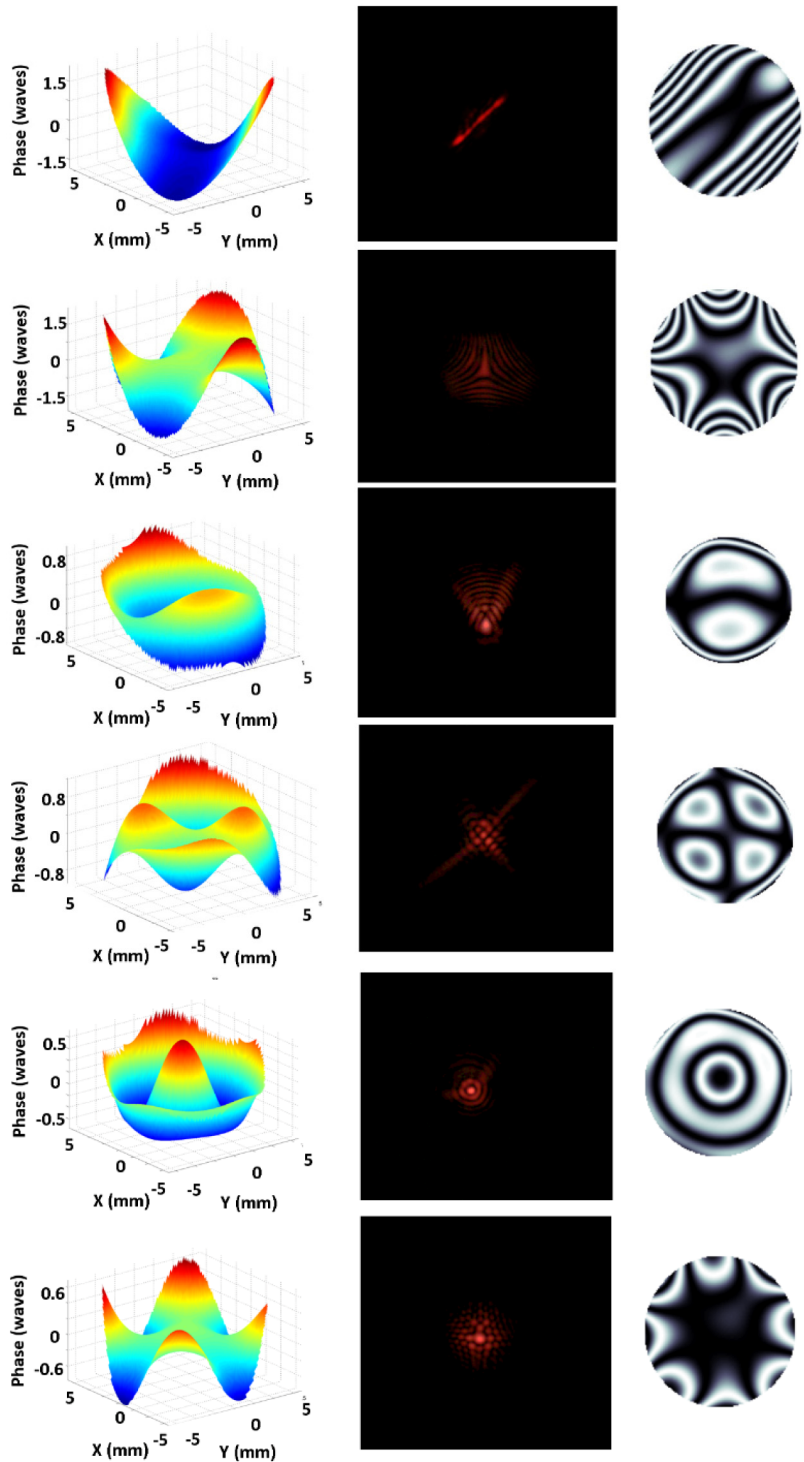


Fig. 4. Measurement of the generation of wavefronts and the far field of the 4th order Zernike polynomials. Note that astigmatism has been summed with defocus to generate a cylindrical wavefront. The third column reports the wavefront represented as an interferogram.

Figure 4 shows the measurements of the wavefronts obtained by the M-AL and their corresponding far fields. Table 1 reports the maximum peak-to-trough amplitude of the Zernike polynomials that can be generated in the closed loop configuration. In order to simulate the contribution of any additional aberration that one would like to correct, a phase plate was inserted in the beam path in front of the M-AL. As reported in Fig. 5 the phase plate introduced mainly a cylindrical wavefront composed of defocus (Z_{20}) and astigmatism (Z_{2-2}) with a total of 0.64 waves rms deviation. Both the far field and wavefront interferogram relative to the aberration of the phase plate are presented in Fig. 4. The effect of the lens correction on image formation was evaluated by trans-illumination of a sample using a visible light source. The sample consisted of a microscope slide prepared with a Tilia Stem cross section. Figure 5 and the movie ([Visualization 1](#)) illustrate the image of the sample acquired before correction, and after correction of the additional aberrations introduced by the phase plate.

Table 1. Measured Peak to Valley amplitude of the Zernike polynomials which is possible to generate with the adaptive lens (measured at 670 nm)

Aberration	Zernike order	PtV(μm)
Tilt	Z_{11}, Z_{1-1}	3
Defocus	Z_{20}	3.8
Astigmatism	Z_{22}, Z_{2-2}	7.7
Coma	Z_{31}, Z_{3-1}	2.2
Trefoil	Z_{33}, Z_{3-3}	2.9
Spherical Ab.	Z_{40}	0.5
Secondary Ast.	Z_{42}, Z_{4-2}	0.75
Quadrifoil	Z_{44}	1.2

2.3 Multi-actuator adaptive lens for Fourier domain optical coherence tomography

Significant progress has been made in using adaptive optics for ophthalmic imaging with wide field fundus photography, confocal scanning laser ophthalmoscopy (cSLO), and optical coherence tomography (OCT) [21–23]. In order to demonstrate the potential for ophthalmic imaging, the M-AL was integrated into a custom-built high speed Fourier Domain (FD) OCT system designed for imaging the mouse retina [17,24]; a schematic of the system is presented in Fig. 6. Light was focused by an external objective (which defines the system’s diffraction-limited resolution) through a cornea flattened with a viscous gel. The adaptive lens was placed adjacent to the objective lens ($f = 25 \text{ mm}$, $\text{NA} = 0.26$), modifying the wavefront and assisting with the focal spot formation at the mouse retina. The FD OCT engine consisted of a 180 nm bandwidth superluminescent light source centered at 860 nm, and a CMOS (Basler Sprint) line scan detector. The optical power at the sample was $750 \mu\text{W}$, and the acquisition rate was 100,000 A-scans per second. The chromatic aberration introduced by the M-AL can be approximated as the one introduced by a glass window of the same thickness of the M-AL and with the same dispersion of the liquid inside the lens. In the presented case of OCT it is negligible because of the low dispersion over the bandwidth of the OCT source (about $\Delta n = 0.0025$).

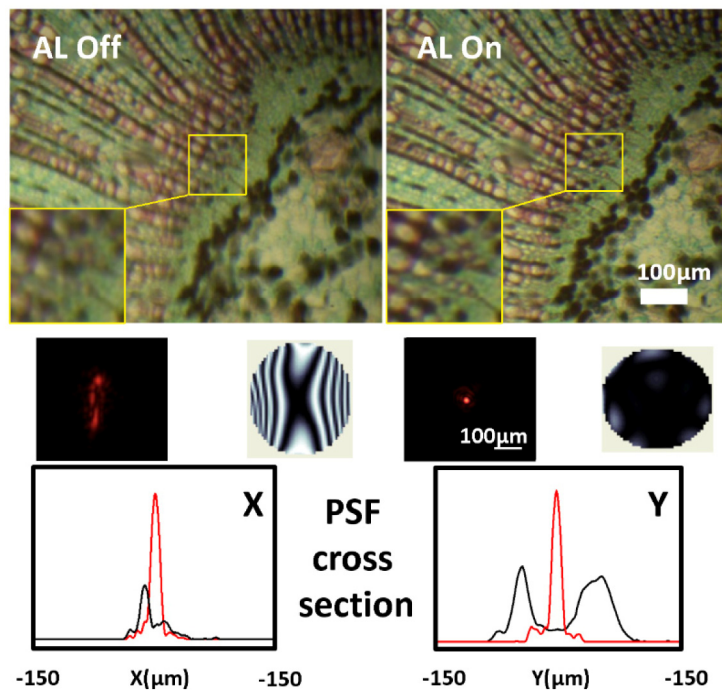
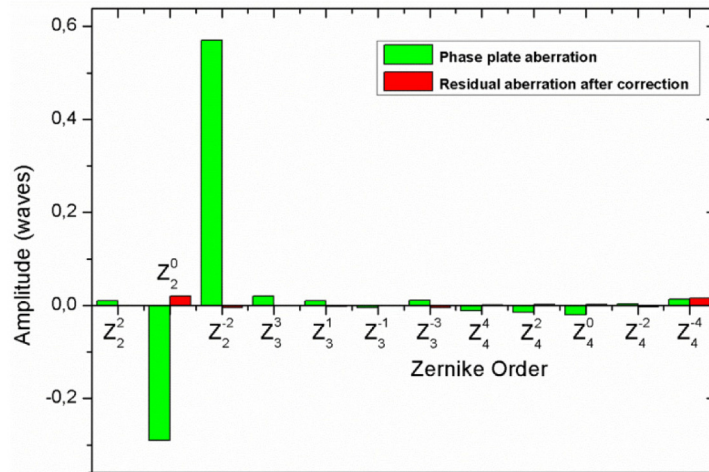


Fig. 5. Top panel: Zernike polynomial decomposition of the aberration introduced by the phase plate, with the adaptive lens flattened with the closed loop, and of the residual aberration after correction. Middle panel: image before and after closed loop correction and (Visualization 1) the image sequence during the closed loop correction. The yellow insets show the central part magnified of two times. Bottom panel: Point Spread Function (PSF), PSF X and Y cross section before (black) and after (red) the correction and wavefront represented as an interferogram.

Unlike the traditional method of adaptive optics which employs a Shack-Hartmann wavefront sensor, we used a wavefront-sensorless approach to correct aberrations in images acquired through the adaptive lens in a mouse FD OCT system [25]. Wavefront sensing in the mouse eye is challenging due to multiple reflections arising from different retinal layers [26]. Although Shack-Hartmann wavefront sensing has been demonstrated for adaptive optics imaging of pigmented mice [24,27], this technique does not work for albino animals in which

backscattered light from the relatively thick and diffusively scattering choroid is a dominant signal. Wavefront-sensorless aberration correction overcomes these limitations by removing the wavefront sensor, and instead optimizing the shape of the deformable element based on changes in image quality. Low order aberration correction for wavefront-sensorless adaptive optics multiphoton fluorescence imaging of mouse retina has recently been reported [28,29]. In our implementation of wavefront-sensorless aberration correction for adaptive optics FD OCT, an image quality based metric (intensity) was used to iteratively tune the shape of the adaptive lens with an algorithm that optimizes each term of the Zernike polynomial describing the shape of the wavefront aberrations to be corrected. By extracting an *en face* plane of the FD OCT volume data for measurement of the image quality metric, we were able to perform aberration correction at an arbitrarily selected depth in the sample that corresponded to the retinal layer of interest. Details on the wavefront-sensorless FD OCT system using a deformable mirror are presented elsewhere [17].

Unlike deformable mirror-based adaptive optics systems in which the deformable element is optically conjugated to the pupil plane (objective lens), the adaptive lens was placed adjacent to the objective lens, reducing the length of the optical path and decreasing the sensitivity to misalignment errors. The use of lenses (instead of curved mirrors) also contributed to the ease of alignment and a smaller footprint, both of which are valuable for clinical applications in retinal high-resolution imaging with adaptive optics [26].

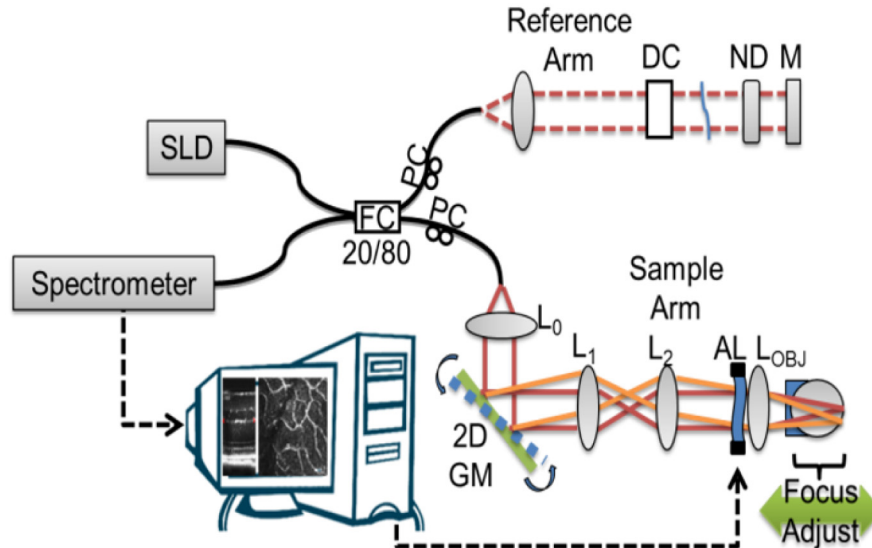


Fig. 6. System topology of the compact wavefront-sensorless Adaptive Lens FD OCT system (L_{OBJ}, 25 mm focal length lens; NA = 0.26). SLD, superluminescent diode; PC, polarization controller; DC, dispersion compensation; ND, neutral density filters; M, mirror; 2D GM, x and y galvanometer mounted mirrors were separated by a telescope but are shown combined for convenience; AL, adaptive lens.

2.4 AO-OCT Results

The numerical aperture of the imaging system was 0.26, corresponding to a focal spot waist of 2.1 μm . Manual adjustment was used to align the focus to the retinal nerve fiber layer, and a representative *en face* projection of a volume image acquired with the adaptive lens in the neutral position is presented in [Fig. 7(a)]. The identically processed image acquired at the same location after aberration correction using the wavefront-sensorless algorithm to control the shape of the adaptive lens is presented in [Fig. 7(b)]; the values of the merit function in response to the bias aberrations of the Zernike polynomial coefficient applied to the adaptive

lens for wavefront correction are presented in [Fig. 7(c)]. With the aberration correction from the adaptive lens, the overall intensity of the image is increased, and features are sharper.

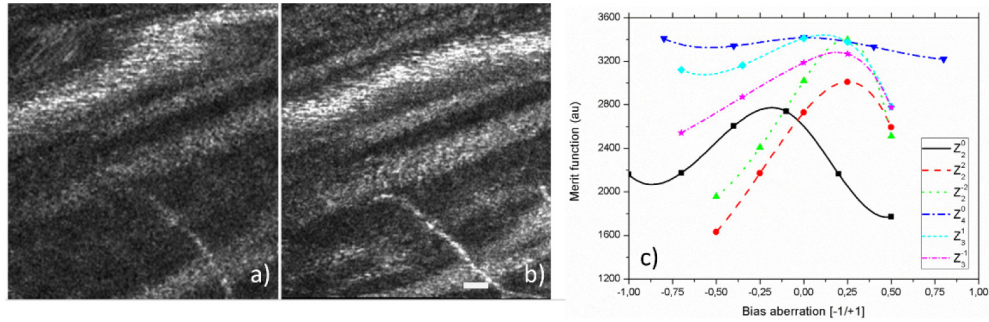


Fig. 7. Adaptive Lens FD OCT images of mouse nerve fiber layer *in vivo* before a) and after b) the adaptive lens optimization. c) Merit function progression during the wavefront-sensorless optimization process. Scale bar: 20 μ m.

3. Discussion

In this report, we presented a new type of refractive wavefront modulator and describe its advantages for use in high resolution *in vivo* imaging of mouse retina. In comparison to other refractive wavefront modulators the M-AL is polarization insensitive and can operate with broadband sources. The present Multi actuators Adaptive Lens is able to correct wavefront aberrations up to the 4th Zernike polynomial order. The piezoelectric actuator elements on the adaptive lens are arranged in rings on the front and back glass surfaces of a liquid-filled cavity, and surround the clear aperture. The performance of the adaptive lens was demonstrated in a straightforward closed loop system using a Shack-Hartmann wavefront sensor. The adaptive lens design is scalable to a larger aperture, and future developments will include the use of anti-reflection coatings and liquids with broadband transmission and low dispersion, along with index matching with the windows material. The prototype M-AL used in the experiments reported here used mineral oil, which has almost no absorption in the visible (NIST Standard Reference Material 1922), and the overall transmittance is about 90%, with losses arising from Fresnel reflections at uncoated surfaces. Future developments include the realization of prototypes able to work in different spectral ranges including the UV and IR, where liquid crystals cannot work, by the use of commercially available oils, glasses and anti-reflection coatings. The wavefront modulation can be further increased by the use of higher voltages in the forward polarization of the PZT actuators and by the use of oils with a higher refractive index.

An advanced imaging application for the M-AL was demonstrated through integration with the objective of a FD OCT system that was customized for *in vivo* imaging of the mouse retina. We acquired images of the retinal nerve fiber layer in a mouse eye with a lens-based FD OCT, combining the adaptive lens combined with the final focusing objective lens. This configuration eliminated the need for folded relay optics to place the deformable element at an optical conjugate of the pupil plane. Integrating the adaptive lens with wavefront-sensorless aberration correction enabled the design of a compact system that is robust to back reflection and misalignment. Further development in the acquisition speed will enable human retinal imaging that combines wavefront-sensorless algorithms and the adaptive lens [17,30]. The performances of the M-AL are compatible for the correction of human eye aberrations with a pupil of 4.5mm [31].

The use of the M-AL should enable the power of adaptive optics to be more widely applied in ophthalmology, microscopy, vision science, small telescopes, free space communication and medium power laser focusing. With well-developed fabrication

techniques, it should be possible to create M-ALs with larger or smaller apertures that can be embedded in microscope and camera objectives or in portable devices, paving the way to new applications or new functionalities of the existing ones. Furthermore, the M-AL, thanks to its ease of use, has the potential to be a new tool for optical designers to increase the performances of diverse complex optical systems.

Acknowledgment

The adaptive lens is patent pending: S. Bonora, TV2014A000014. SB acknowledges the help of Dr. Roberto Piazzesi who has taken part to the early stage of the design and characterization of the adaptive lens. MVS acknowledges support from MSFHR, CIHR, NSERC, FFB, and SFU VPR. RJZ acknowledges support of UC Davis Research Investments in Science and Engineering (RISE) initiative; NIH EY02660 & UC Davis NEI Vision Core Grant.